Quantum-confined Stark effect in Ge/SiGe quantum wells: A tight-binding description

Michele Virgilio and Giuseppe Grosso
NEST-INFM and Dipartimento di Fisica "E. Fermi," Università di Pisa, Largo Pontecorvo 3, I-56127 Pisa, Italy
(Received 14 January 2008; revised manuscript received 26 February 2008; published 9 April 2008)

We present a tight-binding study of the strong quantum confined Stark effect (QCSE) involving direct transitions in Ge/SiGe quantum wells. Our aim is to provide a theoretical and numerical description of the experimental results by Kuo *et al.* [Nature **437**, 1334 (2005)] by means of a tight-binding model. In the presence and in the absence of external electric fields, we are able to assign of the states involved in the observed transitions. Oscillator strengths for normal and parallel incident radiation are evaluated. In particular, the genuine direct transitions in the Ge region, at the Γ point, and the direct transitions coming from states along the Δ lines folded at Γ, are discriminated; their energy shift as a function of a superimposed field is evaluated, and their role in the QCSE is evidenced. Excitonic effects below and above the interband threshold are also included in our calculations; they contribute to a close reproduction of the experimental absorption spectra for different superimposed uniform electric fields.

DOI: 10.1103/PhysRevB.77.165315 PACS number(s): 73.21.Fg, 78.67.De, 71.15.Ap, 32.60.+i

I. INTRODUCTION

Since the observation and interpretation[1,2] of the quantum confined Stark effect (QCSE), it has been evident its potentiality in the design of high performance quantum well optical modulators.[3] The fundamental and technological importance of this effect is testified also by its presence in textbooks on electronic and optical properties of semiconductor nanostructures (see, for instance, Refs. 4–6). For about two decades, the effort to control the strong spectral shifts of the confined direct interband absorption edges with applied electric fields (the QCSE) has been almost exclusively concentrated on III-V semiconductor type-I quantum wells. In fact, the limitation of group IV semiconductors as photonic materials, due to their indirect band gap, prevented their application as light emitting devices. On the other side, never ceased the hope to integrate silicon electronics with silicon-based optoelectronic devices,[7] mainly in telecommunication and interconnection applications.[8]

Only recently, robust QCSE was observed[9–11] in strained Ge quantum wells (QWs) separated by strained $Si_{0.15}Ge_{0.85}$ barriers, coherently grown along the [001] direction on a $Si_{0.1}Ge_{0.9}$ relaxed alloy substrate. For such geometry, the band alignment leads to a type-I profile for the potential around the Γ point of the Ge well where charges are confined. The main idea[9] to realize strong QCSE was to exploit the lowest direct band transition at Γ ($\Gamma_{8v}{}^{+} \rightarrow \Gamma_{7c}{}^{-}$) in compressively strained Ge QWs at about 1500 nm. The result was the detection of a Ge QCSE comparable with that of III-V semiconductors but with the further bonus of being realized with materials compatible with the Si mass-production technology.

In this paper, we present a tight-binding description of the QCSE in the type-I Ge/SiGe quantum well system considered in the experiments reported in Refs. 9 and 10. We reproduce the lowest energy features of the electroabsorption spectrum starting from the band structure of the complete system and including excitonic contributions. In our work, we adopt a first-neighbor $sp^3d^5s^*$ tight-binding Hamiltonian to describe the electronic band structure of the QW system for different values of the electric field orthogonal to the multilayer structure. In Sec. II, we give a few details of the system studied and of the method adopted. Section III contains our results: in particular, we investigate the energy and spatial distribution of the relevant states near the conduction and valence band edges and then the direct interband absorption spectrum is obtained both for parallel and for normal incident radiation. The effectiveness of our tight-binding Hamiltonian description is proven by direct comparison with the experimental measures.[9,10] It is worth noting that our results are not derived by a model band-edge profile as usually happens for calculations based on the effective mass approximation. Indeed, the results reported in the following are based on an atomistic description of the bulk silicon and germanium crystals, and the electronic and optical properties of the QW system are derived starting from the equilibrium position of the atoms composing the strained lattice of the complete heterostructures. Our conclusions are reported in Sec. IV.

II. SYSTEM DETAILS AND THEORETICAL MODEL

The QW heterostructure studied in Refs. 9 and 10 is made of barrier plus well regions periodically repeated ten times, coherently grown along the [001]-crystallographic axis ($\hat{z}$) on a relaxed $Si_{0.1}Ge_{0.9}$ buffer on Si, and eventually capped by a *p*-*i*-*n* diode structure. Each region is composed of a 10 nm wide strained, undoped, Ge well (the active material) and a 16 nm wide strained, undoped, $Si_{0.15}Ge_{0.85}$ barrier. An electric field on the structure is provided by Ohmic Al/Ti contacts evaporated at the bottom and at the top of the heterostructure and is approximately uniform and perpendicular to the QW plane. To model the system, we assume that all the interfaces are perfectly flat and abrupt; the heterostructure is considered infinitely extended along the growth plane. Alloy concentrations are supposed constant and homogeneous within each barrier region. The substrate, buffer, and cap materials have no influence on the optical properties in the near gap energy region (see Ref. 9) and thus are disregarded in our calculations to limit CPU time.

 ©2008 The American Physical Society

To take into account strain effects on the electronic structure, we first calculate the ion positions in the strained lattice. The lattice constants $a_{\perp}$ along the $\hat{z}$ axis in the Ge well and in the barrier layers are evaluated according to the macroscopic elasticity theory.[4,12] Their equilibrium value is determined imposing minimum conditions for the elastic energy within each homogeneous region. They are a function of the Ge content and of the growth plane lattice constant $a_{\parallel}$ which is given by lattice matching with the buffer.[13]

An electric field applied along the growth direction breaks the periodicity of the multiwell structure along the $\hat{z}$ axis, and thus all the layers in the structure should be considered in the calculation. Nevertheless, the spectral properties of each well in the near gap energy range are essentially due to transitions between states that are confined in the Ge layers; features in the absorption spectrum related to less localized electronic states are present only at higher energies. Therefore, in order to limit the number of atomic layers considered in our calculations, we simulate a single Ge well (10 nm) sandwiched between two 8 nm wide $Si_{0.15}Ge_{0.85}$ barriers, assuming periodic conditions along the parallel plane and hard wall conditions at the boundary of the barriers. In this way, the fundamental cell contains less than 2×10^2 atoms, one for each atomic sheet. We have performed the simulation also imposing periodic boundary conditions along the growth direction. i.e., with the uniform electric field substituted by a saw tooth profile linear in each well plus barrier region. Our results for the optical absorption in the near gap region are almost equal in the two cases (see also Ref. 14).

The electronic structure of the system is investigated by means of a first-neighbor tight-binding Hamiltonian with $sp^3d^5s^*$ orbitals and spin-orbit interaction. We adopt the self- and hopping energy parameters obtained by Jancu *et al.*[15] to reproduce the electronic band structure of the bulk silicon and germanium crystals. Linear interpolation with alloy concentration of the tight-binding parameters (virtual crystal approximation) is exploited to describe the $Si_{0.15}Ge_{0.85}$ barrier regions. Although it is well established that electronic states in SiGe alloys are better reproduced by theories beyond the virtual crystal approximation (VCA)[16,17] or numerical supercell calculations,[18] for our purposes, the VCA provides sufficiently accurate results due to the high Ge concentration in the barrier region. Moreover, in our case, the wave functions relevant to the near edge absorption are mainly confined in the pure Ge active material and thus are only weakly sensitive to the alloy disorder in the barriers. Strain effects are accounted for by scaling the hopping parameters according to the laws given in Ref. 15 and evaluating the appropriate modification of the geometrical phase factors of the Hamiltonian matrix.

To model the potential discontinuity at the heterointerfaces between the well and barrier regions, we align their topmost valence band edges by adding a constant potential to the self-energies in the well region. Its value has been evaluated by linear interpolation with alloy concentration of the results reported in Ref. 12 for Si/Ge heterointerfaces under different strain conditions. The constant electric field is modeled adding to the site energies a potential energy linearly varying along the growth direction.

Interband optical absorption for incident light with polarization unit vector $\hat{\epsilon}$ and energy $\hbar\omega$ is evaluated according to the following expression:[19]

$$\alpha(\hbar\omega) = \sum_{c,v} \alpha_{c,v}(\hbar\omega) = \sum_{c,v} \frac{2\pi e^2\hbar}{n_0 c m_0 V\Gamma} \sum_{\vec{k}} \frac{P^{\epsilon}_{c,v}(\vec{k})}{E_c(\vec{k}) - E_v(\vec{k})} \cdot \{f[E_v(\vec{k})] - f[E_c(\vec{k})]\} \cdot \frac{1}{1+\left(\frac{E_c - E_v - \hbar\omega}{\Gamma}\right)^2}, \tag{1}$$

where $P^{\epsilon}_{c,v}(\vec{k})=(2/m_0)|\langle c,\vec{k}|\hat{\epsilon}\cdot\vec{p}|v,\vec{k}\rangle|^2$ is the squared modulus of the dipole matrix element, expressed in eV, between conduction $|c,\vec{k}\rangle$ and valence $|v,\vec{k}\rangle$ states with energies E_c and E_v, respectively. The volume V is equal to the product of the unit area in the QW plane and the width of the Ge plus barrier region. $f(E)$ is the Fermi distribution function; for $T \lesssim 300$ K, we can safely assume $f[E_v(\vec{k})]=1$ and $f[E_c(\vec{k})]=0$. n_0 is the QW refractive index; it is almost independent from the frequency in the energy range of interest. Its value has been chosen equal to the static bulk germanium refractive index. Finally, the Lorentzian distribution is introduced in Eq. (1) to phenomenologically take into account linewidth effects. To reproduce the room temperature data for the peak widths reported in Ref. 10, we set $\Gamma=8$ meV which is the same value adopted in similar calculations.[20] Furthermore, we assume here that the variation of Γ with the electric field strength can be neglected. This is supported by the invariance of the measured absorption peak widths for different field strengths.[10] The sum over $\vec{k}$ in Eq. (1) is evaluated sampling the two-dimensional Brillouin zone with 200 independent $\vec{k}$ points along the [100] direction. The length of the sampled segment is chosen so that all the *direct* transitions below a given energy threshold are considered. In this way, in the evaluation of near gap absorption spectra, we take into account transitions between QW confined states, their different dispersions around the gamma point, and also contributions at higher energies involving less localized states extending into the barriers (see Figs. 2 and 3).

To evaluate the matrix elements $|\langle c,\vec{k}|\hat{\epsilon}\cdot\vec{p}|v,\vec{k}\rangle|$ of the momentum operator between valence and conduction states, we follow the procedure originally introduced by Ren and Harrison[21] for the evaluation of the optical properties of bulk semiconductors with the tight-binding method. The same approach has been successfully adopted also for tight-binding simulations of nanostructured systems.[22–26] Ren and Harrison[21] have shown that if the basis wave functions are not explicitly known (as is the case for the parametrization of Ref. 15), the dipole matrix elements can be reasonably approximated by the following relation:

$$\langle \phi_i|\vec{p}|\psi_j\rangle \simeq \frac{im}{\hbar}\langle \phi_i|H|\psi_j\rangle \vec{d}_{ij}, \tag{2}$$

where $\vec{d}_{ij}$ is the vector connecting the orbitals ϕ_i and ψ_j, localized on the sites i and j, respectively. We note that the

approximate relation [Eq. (2)] is compatible with gauge invariance and with the $q \to 0$ limit of the equation for charge conservation.[27,28]

For each couple of bands (c,v) involved in expression (1), excitonic contributions are evaluated by means of the two-dimensional Elliott expression,[6]

$$\alpha^{ex}_{c,v}(\hbar\omega) = \alpha_{c,v}(\hbar\omega)\left[\sum_{n=0}^{\infty} \frac{4}{\left(n+\frac{1}{2}\right)^3}\delta\left(\Delta + \frac{1}{\left(n+\frac{1}{2}\right)^2}\right) + \Theta(\Delta)\frac{e^{\pi/\sqrt{\Delta}}}{\cosh\left(\frac{\pi}{\sqrt{\Delta}}\right)}\right], \quad (3)$$

where $\alpha_{c,v}(\hbar\omega)$ is given in expression (1), $\Delta = \frac{\hbar\omega - E_{c,v}}{E_0}$, $E_{c,v}$ is the energy difference of the considered couple of bands at the band edge, and $4E_0$ is the exciton binding energy. The two terms in the square brackets in Eq. (3) account for the below (Rydberg-like) and above (Coulomb enhancement) gap features. Also for the Rydberg states, a line shape Lorentzian broadening is introduced with linewidth of 8 meV. For the excitonic binding energy, we have adopted the value $4E_0 = 3.6$ meV.[10]

III. RESULTS

Before presenting our numerical results for the Ge/SiGe QW heterostructure, it is useful to briefly summarize the most relevant effects on the electronic band structure of SiGe bulk alloys induced by biaxial strain.[29–31] Let us consider the case of a SiGe crystal grown along the [001] direction on a cubic SiGe substrate. If the Ge concentration in the substrate is greater (less) than the Ge concentration in the deposited material, the in-plane strain of the deposited material is tensile (compressive). The tetragonal distortion is at the origin of the topmost valence heavy- and light-hole bands observed at the Γ point. For tensile strained materials, the light-hole band is found at higher energy than the heavy hole. The opposite holds for compressive strained alloy. Also, the minima of the conduction band are modified by strain. Due to the inequivalence of the parallel (in plane) and orthogonal (growth) direction, the six degenerate Δ valleys of the cubic structure become nondegenerate. In fact, in the case of tensile strain, the two $\Delta_\perp$ minima along the [001] and $[00\bar{1}]$ directions have lower energies than the four $\Delta_\parallel$ valleys in the parallel plane. Biaxial compressive strain in Ge-rich alloys lowers the energy difference between the eight L minima and the $\Delta_\parallel$ valleys (the L minima remain degenerate because of the preserved equivalence of the [111] directions). In particular, Ge crystals grown along the [001] direction on SiGe substrates with Ge concentration of less than $\simeq 0.4$ are predicted[30–32] to have the lowest conduction band along the $\Delta_\parallel$ line. All these effects are qualitatively captured and also quantitatively well reproduced by the full-band tight-binding parametrization of Ref. 15.

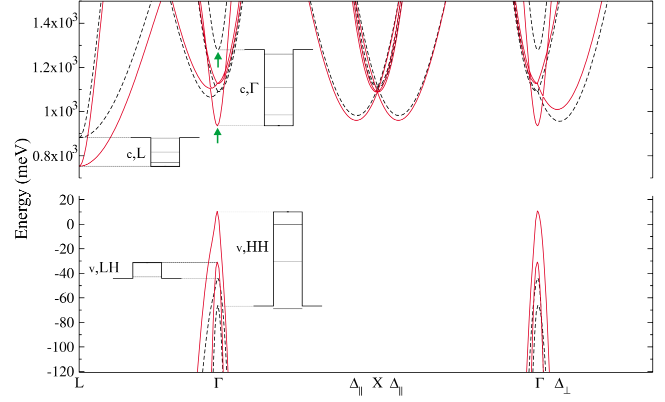

FIG. 1. (Color online) Aligned bulk electronic band structures of isolated strained $Si_{0.15}Ge_{0.85}$ (black dashed lines) and Ge (red continuous lines) crystals composing the barrier and the quantum well region, respectively. $a_\parallel$ is matched with the lattice constant of the $Si_{0.1}Ge_{0.9}$ buffer and the origin of the energy axis has been fixed at the topmost of the QW valence state (HH1). Band-edge profiles for the light- and heavy-hole valence bands and for the L and Γ conduction valleys are sketched together with the evaluated confined levels of the complete QW heterostructure (in the absence of electric fields). Parallel and orthogonal directions are referred to the growth plane. The green arrows indicate the lowest genuine levels at Γ, not originated by folding. Notice that the energy scales for conduction and valence bands are different.

A. Reference system

In order to assign the meaning of the states obtained by diagonalization of the tight-binding Hamiltonian for the complete (well+barriers) system considered in Refs. 9 and 10, it is convenient to preliminary analyze the electronic band structure of the isolated bulk $Si_{0.15}Ge_{0.85}$ alloy under tensile strain conditions and of the isolated bulk Ge crystal under compressive conditions consistent with their growth on a $Si_{0.1}Ge_{0.9}$ alloy buffer. For this aim, we report on the same graph (see Fig. 1) the electronic band structure of the two systems, properly aligned as discussed in the previous section. The relevant band-edge profiles at Γ and L points are also indicated.

As evident from Fig. 1, at the Γ point, the heavy-hole (HH) band edges determine a robust confining profile for holes in the valence, with well deep of $\simeq 77$ meV, while the light-hole (LH) bands provide a well with depth of 13 meV. QW LH states of the complete structure are expected in the -30 to -45 meV energy range (see Fig. 1). For both bulk strained materials, the lowest conduction band occurs at the L point with $E_{c,L}(Si_{0.15}Ge_{0.85}) - E_{c,L}(Ge) \simeq 129$ meV. The $\Delta_\perp$ and $\Delta_\parallel$ valleys have higher energies and are shifted in opposite directions in the Ge and $Si_{0.15}Ge_{0.85}$ materials. Therefore, $\Delta_\parallel$ and $\Delta_\perp$ states localize in the Ge and in the barrier region, respectively. The two genuine lowest conduction states at Γ have been indicated in Fig. 1 by green arrows to distinguish them from the states at Γ (around 1110 meV) originated by the folding of the $X_\perp$ point into Γ. This occurs when a tetragonal Brillouin cell is used to describe the lattice periodicity, as is usual for biaxially strained crystals grown along the [001] direction.[33] We find that in the complete QW het-

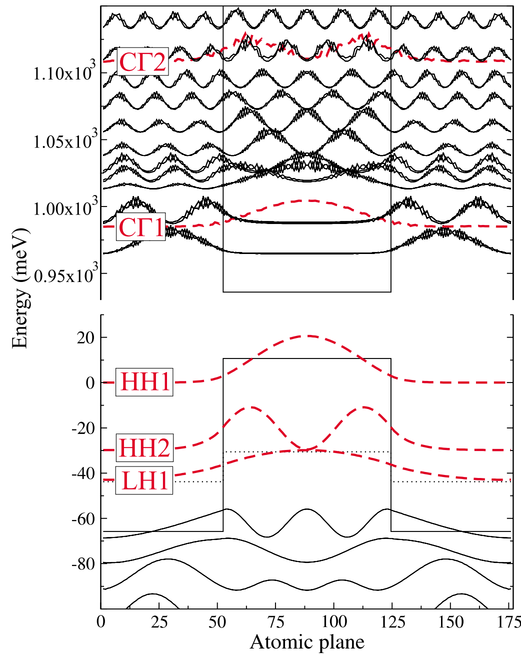

FIG. 2. (Color online) Near gap electron and hole energies and squared wave functions, at Γ, for the unbiased Ge QW (layers from 53 to 125) between $Si_{0.15}Ge_{0.85}$ barriers (layers from 1 to 52 and from 124 to 176). The heavy red dashed lines represent the heavy-hole, the light-hole, and the conduction states confined in the Ge region (not derived by folding at Γ of the $\Delta_\perp$ line). HH (solid), LH (dotted), and conduction (solid) band-edge profiles are also reported. Black solid lines in the conduction represent $\Delta_\perp$ states folded into the Γ point; typical oscillations due to intervalley coupling are visible. For energies greater than 1000 meV, $\Delta_\perp$ states penetrate into the well region. The energy scales for the conduction and valence bands are different. The zero of energy is fixed at the HH1 energy level.

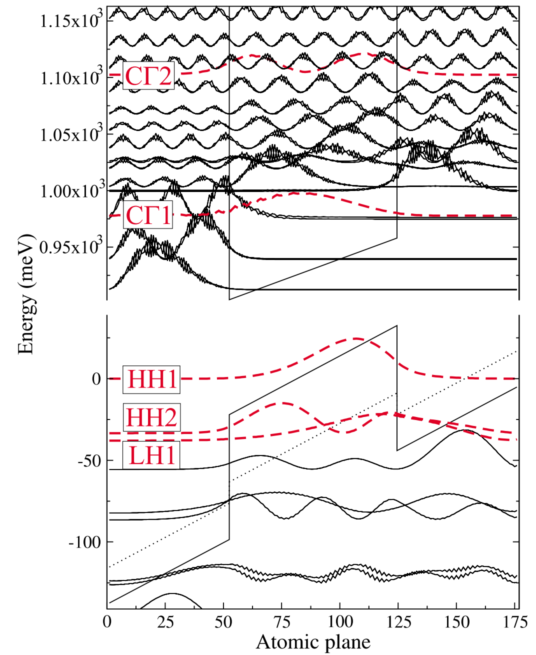

FIG. 3. (Color online) As in Fig. 2 but in the presence of a superimposed electric field of 2 V ($\mathcal{E} \simeq 5 \times 10^4$ V cm^{-1}) along the growth axis.

erostructure, direct optical coupling between QW folded conduction states and valence states at Γ is negligible, as one can expect considering that the related bulk states belong to different $\vec{k}$ values. The bottom conduction band-edge potential at Γ (see Fig. 1) is 183 meV higher than the bottom of the strained Ge conduction band at L. The well depth for electrons at Γ is ≃343 meV; thus, strong confinement of the near gap states at the Γ point is expected.

B. Ge/SiGe quantum well heterostructure

We report here the energy, spatial confinement and symmetry character of the electronic states in the near gap energy region of the complete heterostructure of Refs. 9 and 10, evaluated in the absence and in the presence of applied electric fields. The system considered is composed of a 72 ML (monolayer) Ge QW and a 104 ML SiGe barrier. In Fig. 2, the wave functions, at the Γ point, for the unbiased system are shown. Consistently with band-edge profiles reported in Fig. 1 for the bulk electronic band structures of the strained $Si_{0.15}Ge_{0.85}$ and Ge crystals, we find in the valence the two heavy-hole states and one light-hole state confined in the germanium region. With the zero of energy set at the HH1 state, the HH2 and LH1 levels are at ≃−30 and ≃−43 meV, respectively; the LH2 and HH3 QW states and valence continuum Ge states hybridized with the SiGe barrier states lie at lower energies. The Γ conduction band-edge profile confines three QW subbands, $c\Gamma1$, $c\Gamma2$, and $c\Gamma3$ (not shown in Fig. 2) with energies of 985, 1108, and 1260 meV, respectively. Other confined levels with energy in the range of 960–1090 meV are distinguishable in Fig. 2. These states originate from the folding of the $\Delta_\perp$ line into Γ.[31] Furthermore, their doublet structure and the fast oscillations modulating the envelope functions are a characteristic signature of intervalley interaction as expected for QW states originated from two degenerate bulk valleys.[34–37]

In Fig. 3, we report the near gap states evaluated at the Γ point in the presence of an electric field $\mathcal{E} \simeq 5 \times 10^4$ V cm^{-1} applied along the growth direction, corresponding to an applied potential of 2 V.[9] In this case, only the fundamental $c\Gamma1$ (978 meV) and first excited $c\Gamma2$ (1102 meV) conduction Γ states are fully confined in the Ge region. In the valence band, the HH1 state is almost completely confined in the Ge well, while the HH2 and LH1 states have nonvanishing wave function amplitude also in the right barrier (see Fig. 3). Their energies are −33 and −38 meV, respectively. Comparing the energies of the HH1-$c\Gamma1$ and of the LH1-$c\Gamma1$ transitions of the unbiased and biased QW systems, we obtain for the QCSE energy shifts the values 7 and 12 meV, respectively. These values result from the shift induced by the field on both the valence and conduction QW states.

To evaluate valence and conduction Stark shifts as a function of the field strength, we set the origin of the field potential at the left barrier and/or well heterointerface and calculate the energy shifts for the HH1, LH1, and $c\Gamma1$ QW states with biases in the range of 0–4 V. The results are reported in

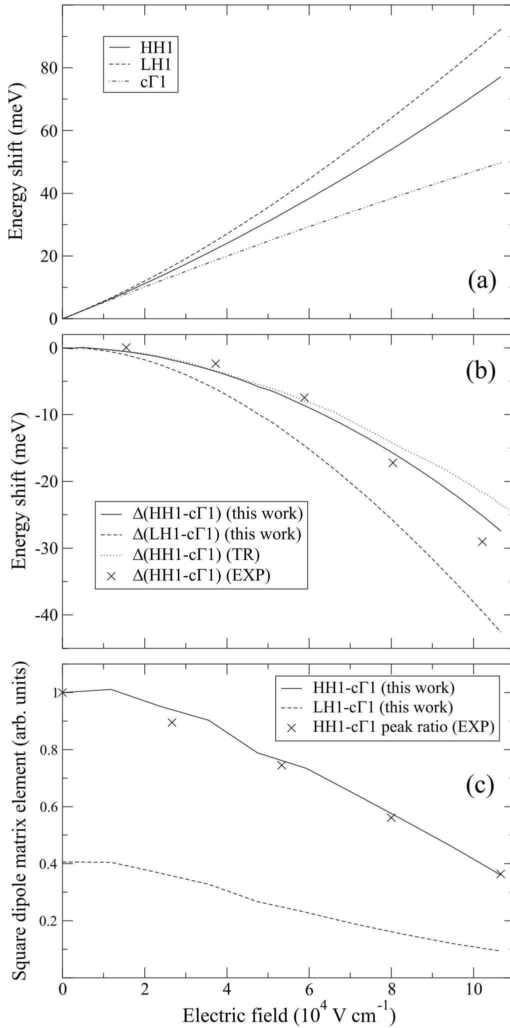

FIG. 4. (a) HH1, LH1, and $c\Gamma 1$ energy shifts as a function of the electric field strength calculated at the Γ point for the QW system discussed in the text. (b) Stark shifts evaluated for the corresponding transitions. Experimental values (expt.) and results from TR simulations for the HH1-$c\Gamma 1$ transition are also reported. Panel (c) shows the field dependence of the square modulus of the dipole matrix elements at Γ for the HH1-$c\Gamma 1$ and LH1-$c\Gamma 1$ transitions at normal incidence. Measured peak intensities for the HH1-$c\Gamma 1$ transition, normalized to the zero field value, are also reported.

Fig. 4(a). The Ge bulk conduction effective mass at Γ is lighter than the effective masses of the HH and LH states at Γ and then the $c\Gamma 1$ confinement energy (49 meV) is greater by a factor of about 5 with respect to the HH1 (10 meV) and LH1 (12 meV) confinement energies (see Fig. 2). For this reason, the $c\Gamma 1$ level is less sensitive to the bending of the QW bottom induced by the field and its Stark shift is smaller. Therefore, the net shifts for the HH1-$c\Gamma 1$ and LH1-$c\Gamma 1$ transitions are negative as it happens for QCSE based on III-V compounds.[38] This is shown in Fig. 4(b) together with the experimental measurements,[9,10] and a theoretical prediction based on tunneling resonance (TR) calculations also reported in Refs. 9 and 10. The overall agreement between measured and our theoretical values is good. We also confirm the quadratic dependence of the QCSE on the field strength as proposed in Ref. 38 by means of a variational approach. Note also that the QCSE for the LH1-$c\Gamma 1$ transition is greater than for the HH1-$c\Gamma 1$ one. This is due to the less robust offset of the LH band-edge profile, which is responsible of the greater shift of the wave function barycentre toward the right barrier (see Fig. 3). In fact, in the presence of a field along the growth axis, the barycenters of the valence and conduction confined wave functions move in opposite directions and their spatial overlap diminishes. As a consequence, also the dipole matrix elements of the HH1-$c\Gamma 1$ and LH1-$c\Gamma 1$ transitions diminish and the related absorption peaks are weakened. Because of the proportionality between the square dipole matrix elements and the peak intensities, we can directly compare their variations as a function of the field strength. The agreement between experimental and theoretical data is very satisfactory as shown in Fig. 4(c).

Our results for absorption spectra under, different bias conditions, for parallel and normal incident radiation, are reported in Figs. 5(a)–5(e). For comparison, experimental results at normal incident radiation are also reported. Measurements have been performed at room temperature, while our theoretical predictions are based on the tight-binding parametrization of Ref. 15 which has been deduced in the low temperature regime. We have thus considered the temperature correction of the energy gap redshifting all the calculated spectra by 104 meV. This value has been chosen to fit the measured spectrum at $V=0$, and it is compatible with the semiempirical law given in Ref. 39 which describes the temperature dependence of the direct transition in a QW Ge system composed of a similar number of monoatomic layers.

For normal incident radiation, the overall agreement between our results and the experimental spectra is quite satisfactory and allows assignment of the experimental features. Near gap peaks, positions and Stark shifts are qualitatively and quantitatively well reproduced as due to the HH1-$c\Gamma 1$ and LH1-$c\Gamma 1$ transitions. Also, the calculated widths and intensities of the HH1-$c\Gamma 1$ and LH1-$c\Gamma 1$ absorption features agree with the experimental data.

The importance of excitonic contributions in the interpretation of experiments is evident from the comparison with the bare interband absorption $\alpha(\hbar\omega)$ given by Eq. (1) (see Fig. 5). We also stress that the break of the QW symmetry by the electric field in the growth direction greatly influences optical selection rules. In fact, in the absence of external fields and for normal incidence, only HH$n \rightarrow c\Gamma n$ and LH$n \rightarrow c\Gamma n$ transitions are allowed.[40] In the presence of the field, also HH$n \rightarrow c\Gamma m$ and LH$n \rightarrow c\Gamma m$ transitions with $n \neq m$ become allowed, contributing to the overall shape of the spectrum. This is confirmed by the calculated dipole matrix elements which are reported in Fig. 5 by vertical bars.

Since the Stark shifts of the LH1-$c\Gamma 1$ transition are larger than the one of the HH1-$c\Gamma 1$ transition [see Fig. 4(b)], it is interesting to evaluate the absorption spectra for incident radiation parallel to the QW plane. In fact, in this case, the HH1-$c\Gamma 1$ transition is depressed for symmetry reasons[40] and the absorption threshold is governed by the allowed LH1-$c\Gamma 1$ transition; strong modulation of the absorption can thus be realized also by parallel incident radiation. Our numerical results for parallel incident radiation are shown in Figs. 5(a)–5(e); they show negligible absorption at the

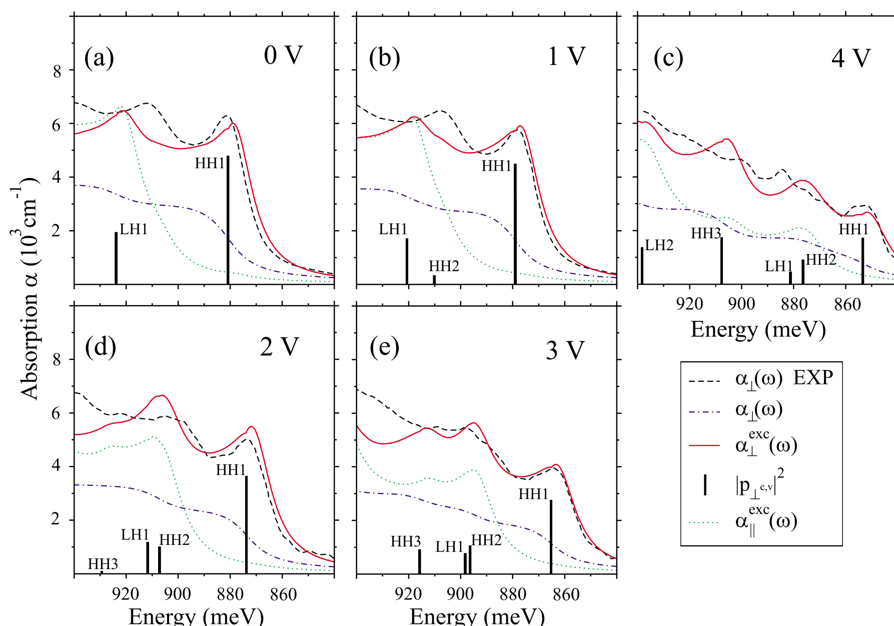

FIG. 5. (Color online) Experimental and theoretical near gap absorption spectra at room temperature under different bias voltages. For normal incidence, we report experimental data (back dashed lines), numerical absorption evaluated with (red solid line) and without (blue dot-dashed line) excitonic contributions, and square modulus of the optical matrix elements (vertical bars). The label on the vertical bars indicates the starting state of the transition; the final state is $c\Gamma1$. The absorption excitonic spectrum evaluated for parallel incident radiation is also reported (green dotted line).

HH1-$c\Gamma1$ energy and robust Stark shift of the absorption edge.

IV. CONCLUSIONS

We have performed numerical investigations of the confined Stark effect in strained Ge quantum wells separated by $Si_{0.15}Ge_{0.85}$ barriers. Our simulations support the experimental results of Ref. 9 that this effect is robust even in group IV heterostructures involving Ge QWs provided that direct transitions at Γ are exploited. By a nearest neighbor $sp^3d^5s^*$ tight-binding model, we have evaluated the electronic states of the complete structure (well plus barriers) and their energy shifts in the presence of a uniform electric field along the growth axis. The atomistic model adopted allows to fully consider spin-orbit interaction, strain in the different regions of the structure, finite band offsets at the heterointerfaces, and alloying.

The role of states along the $\Delta_\perp$ lines reported at Γ due to the Brillouin zone folding has been evidenced. The tight-binding model also allows the evaluation of the absorption coefficients considering all the states in the Brillouin zone contributing to the spectrum up to a chosen energy; excitonic contributions have also been inserted in the model leading to a close reproduction and interpretation of the measured spectra. The role of the polarization of the incident radiation has been analyzed. This work shows that the tight-binding model is most adequate for the description of the QCSE and in the design of group IV multilayer structures for optoelectronic devices.

ACKNOWLEDGMENTS

We thank S. M. Goodnick for helpful discussions. This work has been supported by National Enterprise for Nano-Science and NanoTechnology (NEST).

[1] D. A. B. Miller, D. S. Chemla, T. C. Damen, A. C. Gossard, W. Wiegmann, T. H. Wood, and C. A. Burrus, Phys. Rev. Lett. **53**, 2173 (1984).

[2] D. A. B. Miller, D. S. Chemla, T. C. Damen, A. C. Gossard, W. Wiegmann, T. H. Wood, and C. A. Burrus, Phys. Rev. B **32**, 1043 (1985).

[3] D. A. B. Miller, J. S. Weiner, and D. S. Chemla, IEEE J. Quantum Electron. **22**, 1816 (1986).

[4] J. Singh, *Electronic and Optoelectronic Properties of Semiconductor Structures* (Cambridge University Press, Cambridge, 2003).

[5] P. Harrison, *Quantum Wells, Wires and Dots* (Wiley, Chichester, 2005).

[6] H. Huang and S. Kock, *Quantum Theory of the Optical and Electronic Properties of Semiconductors* (World Scientific, Singapore, 1990).

[7] L. Pavesi, J. Phys.: Condens. Matter **15**, R1169 (2003).

[8] See, for instance, J. E. Roth, O. Fidaner, R. K. Schaevitz, Yu.-H. Kuo, T. I. Kamins, J. S. Harris, and D. A. B. Miller, Opt. Express **15**, 5851 (2007), and reference therein.

[9] Y.-H. Kuo, Y. K. Lee, Y. Ge, S. Ren, J. E. Roth, T. I. Kamins, D. A. B. Miller, and J. S. Harris, Nature (London) **437**, 1334 (2005).

[10] Y.-H. Kuo, Y. K. Lee, Y. Ge, S. Ren, J. E. Roth, T. I. Kamins, D. A. B. Miller, and J. S. Harris, Jr., IEEE J. Sel. Top. Quantum Electron. **12**, 1503 (2006).

[11] S. Tsujino, H. Sigg, and G. Mussler, Appl. Phys. Lett. **89**, 262119 (2006).

[12] C. G. Van de Walle and R. M. Martin, Phys. Rev. B **34**, 5621 (1986).

[13] M. Virgilio, R. Farchioni, and G. Grosso, J. Appl. Phys. **99**, 053710 (2006).
[14] D. P. Barrio, M. L. Glasser, V. R. Velasco, and F. Garcia-Moliner, J. Phys.: Condens. Matter **1**, 4339 (1989).
[15] J.-M. Jancu, R. Scholz, F. Beltram, and F. Bassani, Phys. Rev. B **57**, 6493 (1998).
[16] S. Krishnamurthy, A. Sher, and A.-B. Chen, Phys. Rev. B **33**, 1026 (1986).
[17] R. J. Lempert, K. C. Hass, and H. Ehrenreich, Phys. Rev. B **36**, 1111 (1987).
[18] T. B. Boykin, N. Kharche, G. Klimeck, and M. Korkusinski, J. Phys.: Condens. Matter **19**, 36203 (2007).
[19] *Intersubband transitions in Quantum Wells*, edited by E. Rosencher, B. Vinter, and B. F. Levine (Plenum, New York, 1992).
[20] T. Fromherz, M. Meduna, G. Bauer, A. Borak, C. V. Falub, S. Tsujino, H. Sigg, and D. Grützmacher, J. Appl. Phys. **98**, 044501 (2005).
[21] S. Y. Ren and W. A. Harrison, Phys. Rev. B **23**, 762 (1981).
[22] F. Trani, G. Cantele, D. Ninno, and G. Iadonisi, Phys. Rev. B **72**, 075423 (2005).
[23] L. Brey and C. Tejedor, Solid State Commun. **48**, 403 (1983).
[24] C. Tserbak, H. M. Polatoglou, and G. Theodorou, Phys. Rev. B **47**, 7104 (1993).
[25] M. Virgilio and G. Grosso, J. Appl. Phys. **100**, 093506 (2006).
[26] M. Virgilio and G. Grosso, Nanotechnology **18**, 075402 (2007).
[27] M. Graf and P. Vogl, Phys. Rev. B **51**, 4940 (1995).
[28] T. B. Boykin and P. Vogl, Phys. Rev. B **65**, 035202 (2001).
[29] D. J. Paul, Semicond. Sci. Technol. **19**, R75 (2004).
[30] F. Schäffler, Semicond. Sci. Technol. **12**, 1515 (1997).
[31] M. Virgilio and G. Grosso, J. Phys.: Condens. Matter **18**, 1021 (2006).
[32] M. M. Rieger and P. Vogl, Phys. Rev. B **48**, 14276 (1993).
[33] T. B. Boykin, N. Kharche, and G. Klimeck, Phys. Rev. B **76**, 035310 (2007).
[34] G. Grosso, G. Pastori Parravicini, and C. Piermarocchi, Phys. Rev. B **54**, 16393 (1996).
[35] T. B. Boykin, G. Klimeck, M. Friesen, S. N. Coppersmith, P. von Allmen, F. Oyafuso, and S. Lee, Phys. Rev. B **70**, 165325 (2004).
[36] M. Virgilio and G. Grosso, Phys. Rev. B **75**, 235428 (2007).
[37] A. Valavanis, Z. Ikonić, and R. W. Kelsall, Phys. Rev. B **75**, 205332 (2007).
[38] G. Bastard, E. E. Mendez, L. L. Chang, and L. Esaki, Phys. Rev. B **28**, 3241 (1983).
[39] Y. Yin, D. Yan, F. H. Pollak, M. S. Hybertsen, J. M. Vandenberg, and J. C. Bean, Phys. Rev. B **52**, 8951 (1995).
[40] G. Bastard, *Wave Mechanics Applied to Semiconductor Heterostructures* (Les Editions de Physique, Les Ulis, 1988).